Original Article

A modified sampling method for the precise detection of prostate cancer tissues using a three-dimensional stereotaxic location technique

Wei Li[1#]^, Zhixin Ling[1#], Xin Chen[1#], Chaozhong Wang[1], Yunjie Guo[1], Jie Bao[2], Renpeng Huang[3], Xuedong Wei[1]

[1]Department of Urology, The First Affiliated Hospital of Soochow University, Suzhou, China; [2]Department of Imaging, The First Affiliated Hospital of Soochow University, Suzhou, China; [3]Department of Pathology, The First Affiliated Hospital of Soochow University, Suzhou, China

Contributions: (I) Conception and design: W Li, X Wei; (II) Administrative support: W Li, X Wei, R Huang, Z Ling, X Chen; (III) Provision of study materials or patients: W Li, X Chen, C Wang, J Bao; (IV) Collection and assembly of data: W Li, Y Guo; (V) Data analysis and interpretation: W Li, X Chen, Y Guo; (VI) Manuscript writing: All authors; (VII) Final approval of manuscript: All authors.

[#]These authors contributed equally to this work.

Correspondence to: Xuedong Wei, MD. Department of Urology, The First Affiliated Hospital of Soochow University, 899 Pinghai Road, Suzhou 215006, China. Email: wxd0422@163.com; Renpeng Huang, MD. Department of Pathology, The First Affiliated Hospital of Soochow University, 899 Pinghai Road, Suzhou 215006, China. Email: rphuang@126.com.

Background: The rapid and accurate acquisition of prostate cancer pathological tissue is critical to prostate cancer research but has traditionally proven challenging. However, the gradual application of three-dimensional (3D) modeling in medical practice has overcome many of the related limitations. This cohort study aimed to compare the difference between a 3D stereotaxic sampling method and traditional cognitive sampling method to clarify the factors affecting sampling.

Methods: An analysis of 111 men who received radical prostatectomy for prostate cancer at The First Affiliated Hospital of Soochow University between November 2020 and April 2022 was conducted. The positive rate of the cognitive sampling method and the 3D stereotaxic sampling method and their respective influencing factors, such as age, body mass index (BMI), prostate-specific antigen (PSA), PSA density (PSAD), International Society of Urological Pathology (ISUP) grade, tumor volume, number of positive needles from perineal puncture, clinical T stage, and tumor image location, were compared and analyzed, and a cohort study was conducted.

Results: Among the 111 patients, there were 57 cases of cognitive sampling and 54 cases of 3D stereotaxic sampling. In this study, the positive rate of cognitive sampling was 29.82% (17/57,), and the positive rate of 3D stereotaxic sampling was 61.11% (33/54), with the positive rate of 3D stereotaxic sampling being significantly higher than that of cognitive sampling (P=0.001). In cognitive sampling, tumor volume [odds ratio (OR) =1.10; 95% confidence interval (CI): 1.02–1.20], number of positive biopsy cores (OR =1.30; 95% CI: 1.06–1.60), Prostate Imaging Report and Data System (PI-RADS) score (OR =5.54; 95% CI: 1.60–19.12), and clinical T stage (OR =2.36; 95% CI: 1.31–4.25) were identified as influencing factors; in 3D stereotaxic sampling, these influencing factors were eliminated, with ORs of 1.22 (95% CI: 0.78–1.90), 0.88 (95% CI: 0.72–1.09), 1.09 (95% CI: 0.62–1.92), and 1.51 (95% CI: 0.86–2.65), respectively, representing a statistically significant difference (P<0.05).

Conclusions: The 3D stereotaxic sampling method can accurately obtain the required prostate cancer

^ ORCID: 0000-0002-8009-5542.

tissue from the prostate *in vitro* within a short time, and the factors affecting the positive rate of sampling can be eliminated.

Keywords: Multiparameter magnetic resonance; three-dimensional stereotaxic (3D stereotaxic); prostate cancer; sampling method

Submitted Dec 23, 2023. Accepted for publication Jul 02, 2024. Published online Aug 28, 2024.
doi: 10.21037/qims-23-1820
View this article at: https://dx.doi.org/10.21037/qims-23-1820

Introduction

The acquisition of prostate cancer tissues is an essential part prostate cancer research. The methods for obtaining prostate cancer tissue in the clinic include puncture biopsy, transurethral resection (TUR), and radical prostatectomy, but these methods have obvious disadvantages. At present, the standard 12-core system puncture biopsy protocol has become the mainstream protocol for the initial diagnosis and grading of prostate cancer (1). However, the amount of prostate cancer tissue obtained through prostate puncture biopsy is very small and cannot meet the scientific requirements for large projects and multicenter research. An increase in the number of core areas (to 18–24 core areas) for punctures, in what is termed the saturation puncture method, has been proposed for tumor detection (2). However, related studies have suggested that increasing the number of prostate puncture cores does not significantly improve the detection rate of prostate cancer and increases the incidence of prostate puncture-related complications, such as infection and bleeding (3). Thus, for obtaining a sufficient amount of fresh prostate cancer tissues, prostate puncture biopsy is not a reasonable choice. The TUR of prostate specimens is a common approach for obtaining tissues of incidental prostate cancer, but it is not reliable for the accurate detection of prostate cancer (4). Currently, prostate cancer tissues are more frequently obtained from radical prostatectomy specimens. However, unlike gastric cancer, bladder cancer, and kidney cancer, which can be observed with the naked eye after gross specimen resection, prostate cancer is characterized by endogenous infiltration and growth that are often scattered in multiple foci and generally does not produce cancerous interstitial reactions. Therefore, when the specimen is removed, the naked eye still cannot distinguish prostate cancer tissue from surrounding normal tissues (5). Moreover, the proteomics and RNAomics research of prostate cancer has high requirements for the freshness and integrity of specimens. A too-long storage time and routine pathological specimen preparation process will lead to the destruction of RNA and other materials (6), thus rendering the desired research impossible.

Multiparametric magnetic resonance imaging (mpMRI) improves the detection rate of clinically significant prostate cancer and provides valuable information on the histopathological aggressiveness of prostate cancer foci (7). Drost *et al.* (8) and Klotz *et al.* (9) suggested that prostate puncture biopsy under the guidance of mpMRI can improve the diagnostic accuracy of clinically significant prostate cancer.

The current three-dimensional (3D) technology comprises two elements—3D printing technology and 3D image modeling technology—and has been well integrated into surgical practice and research, with 3D modeling being capable of displaying highly intuitive anatomical models (10). Shin *et al.* verified the tumor location of targeted needle biopsy through 3D printing models and guided radical prostatectomy with nerve preservation (11).

However, the means to initially acquiring tumor tissue as accurately as possible from the isolated prostate is still lacking. Given the advantages of mpMRI and 3D technology for the diagnosis and treatment of prostate cancer, this study aimed to develop a specific prostate tumor marking device to locate the true boundary of the prostate cancer in fresh prostatectomy specimen. In this manner, we sought to obtain a sufficient amount of tumor tissue within a short period of time. The results of this study will help in more precisely obtaining prostate cancer tumor tissue from isolated prostates and meet the demand for fresh specimens in prostate cancer research. We present this article in accordance with the STROBE reporting checklist (available at https://qims.amegroups.com/article/view/10.21037/qims-23-1820/rc).

Methods

Ethical approval

This study was conducted in accordance with the

Table 1 Baseline characteristics of the patients with prostate cancer enrolled in this study

Variable	Cognitive sampling (N=57)	3D stereotaxic sampling (N=54)	P
Age (years)	71±5.8	69±5.7	0.124
BMI (kg/m^2), n (%)			0.08
<18.5	1 (1.8)	4 (7.4)	
18.5–23.9	27 (47.3)	24 (44.4)	
24–28	18 (31.6)	23 (42.6)	
>28	11 (19.3)	3 (5.6)	
ISUP score, n (%)			0.05
1	1 (1.8)	4 (7.4)	
2	18 (31.6)	20 (37)	
3	21 (36.8)	21 (38.9)	
4	6 (10.5)	6 (11.1)	
5	11 (19.3)	3 (5.6)	
PI-RADS score, n (%)			0.54
≤3	16 (28.1)	18 (33.4)	
4	21 (36.8)	17 (31.5)	
5	20 (35.1)	19 (35.1)	
Image position, n (%)			0.24
PZ	41 (71.9)	35 (64.8)	
TZ	13 (22.8)	10 (18.5)	
PZ + TZ	3 (5.3)	9 (16.7)	
PSA (ng/mL)	14.9 (7.28–22.48)	10.99 (5.77–20.93)	0.16
PSAD (ng/mL × cm^3)	0.23 (0.12–0.48)	0.15 (0.08–0.31)	0.05
Tumor volume (cm^3)	1.33 (0.41–7.28)	1.19 (0.77–2.66)	0.65

Data are presented as mean ± standard deviation or median (interquartile range). The ages of patients who underwent cognitive sampling and 3D stereotaxic sampling were 71±5.8 and 69±5.7 years, respectively. 3D, three-dimensional; BMI, body mass index; ISUP, International Society of Urological Pathology; PI-RADS, Prostate Imaging Report and Data System; PZ, peripheral zone; TZ, transitional zone; PSA, prostate-specific antigen; PSAD, prostate-specific antigen density.

Declaration of Helsinki (as revised in 2013). All patients were counseled regarding the risks of the procedure and signed an informed consent form that included permission to use their clinical data for research. Ethical approval was obtained from the Institutional Review Board of The First Affiliated Hospital of Soochow University (No. [2022]469).

Clinical trial registration

The study was registered in Chinese Clinical Trial Registry (ChiCTR2300071287).

Patient recruitment

The study was completed at The First Affiliated Hospital of Soochow University (Suzhou, China) from November 2020 to April 2022. A total of 111 male patients attended the hospital for mpMRI examination, prostate biopsy after the diagnosis of prostate cancer, and finally laparoscopic radical prostatectomy. Among these patients, 57 prostate specimens were obtained using the cognitive sampling method and 54 were obtained using the 3D stereotaxic sampling method. The basic information of all patients is shown in *Table 1*; there was no statistically significant

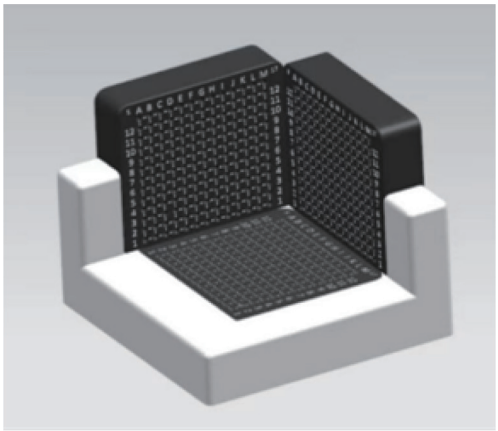

Figure 1 Three-dimensional stereotaxic positioning model.

difference between the two groups.

Magnetic resonance imaging (MRI) acquisition and preoperative prostate biopsy

All patients underwent MRI with a 3-T MR scanner (MAGNETOM Skyra, Siemens Healthineers, Erlangen, Germany). An 18-channel body and standard spinal array coils were used for signal reception. Cross-sectional T1-weighted fast spin echo images of the prostate and seminal vesicles and cross-sectional, coronal, and sagittal T1-weighted fast spin echo images were obtained. Apparent diffusion coefficients were obtained using diffusion-weighted imaging, and the B-values were acquired several times (0, 100, 800, 1,000, and 1,500 $s \cdot mm^{-2}$) using two-dimensional (2D) echo planar imaging sequences. Diffusion-sensitive gradients were applied along the x, y, and z axes. Dynamic contrast-enhanced imaging was performed with a 3D T1-weighted gradient echo volume interpanel gas examination in the same plane as that of the 3D T2W sequence. A contrast agent (Medtronic GMBH, Saarbruecken, Germany) was injected intravenously with a weight of 1 mL/kg at an injection rate of 2.5 mL/s. MR Tissue 4D software (Syngo.Via VA20B; Siemens Healthineers) was used to construct perfusion curves. All patients underwent 12-core transperineal prostatic system biopsy, and the number of positive punctures and corresponding locations was recorded for cognitive sampling.

Software

The 3D modeling software, 3D Slicer, which is an open-source image data analysis and postprocessing platform jointly developed by Harvard University and Massachusetts Institute of Technology, was used to reconstruct human tissues and organs from raw Digital Imaging and Communication in Medicine (DICOM) format data obtained from computed tomography (CT) and MRI. It is compatible with the Windows, Linux, and Mac operating systems and runs smoothly on relatively simple personal computers. By importing prostate data from MRI into 3D Slicer in DICOM medical format for 3D modeling, the volume size of prostate cancer tissue and the boundary of tumor tissue could be obtained through the data measurement module.

Construction of the 3D stereotaxic positioning device

To place the isolated prostate on the sampling plane, a 3D stereotaxic sampling device was designed to locate the prostate tumor tissue through multiple planes. The extractor was composed of a base and two other vertical 3D planes. The three planes had distributions of pinholes at a fixed distance of 5 mm for needle positioning. The isolated prostate could then be placed in an extractor for positioning and sampling. This device has been patented (*Figure 1*).

Sampling methods

Cognitive sampling procedure

We define cognitive sampling as a method of estimating the relative location of tumors in the prostate and sampling them based on a comprehensive analysis of preoperative mpMRI and 12-core system biopsy results. After comprehensive analysis of the tumor location on MRI interpreted by senior radiologists and the location of preoperative positive biopsy, the sampling personnel determined the lesion plane perpendicular to the prostate urethra (consistent with the direction of conventional pathological sections), took a part of the recognized tumor tissue from the plane, and sent it to the pathology department to verify whether it was prostate cancer.

3D stereotaxic sampling procedure

Prostate mpMRI image data were extracted from the picture archiving and communication system before surgery and imported into 3D Slicer software in DICOM format. Experienced radiologists marked the maximum cross-sectional position of the lesion on the MR image (*Figure 2A*), and the same specimen sampler sketched the 3D model at the corresponding position on the 3D Slicer. The position

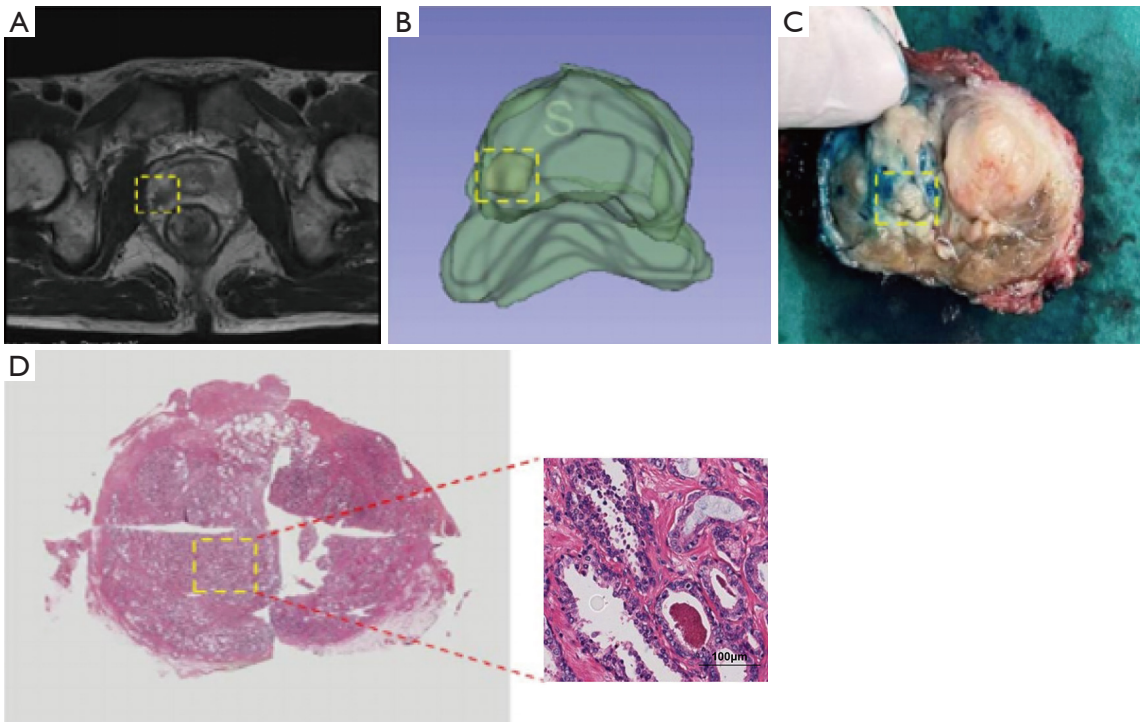

Figure 2 Comparison of the position of the prostate cancer tissue in each stage. The areas of the prostate cancer tissue are indicated by yellow dashed lines. (A) Location of lesions in the mpMRI T2-weighted image. (B) Location of lesions in 3D imaging. (C) Location of lesions as shown in the section of surgical specimen location. (D) Pathology showing the location of the lesions on the sampling surface (the pathological specimens were stained with eosin). mpMRI, multiparametric magnetic resonance imaging; 3D, three-dimensional.

of the lesion relative to the prostate was measured using a tool in 3D Slicer (*Figure 2B*). As described in Section "Construction of the 3D stereotaxic positioning device", according to the structure of the device, the back of the prostate was placed flat in the device so that the urethra was parallel to the underside of the device and the junction of the seminal vesicles and the prostate overlapped with the needle path of the underside of the device. The prostatectomy specimens were fixed through the urethra. According to the measured data, four prostate puncture needles were used to locate the tumor tissue boundary through the puncture hole of the sampling device. A small amount of methylene blue was injected into each puncture needle as it withdrew from the back, leaving four blue needle paths on the prostate plane perpendicular to the urethra. The maximum cross-section profile of the tumor formed by the four blue needle paths was displayed by cutting into the maximum cross-section position plane of the tumor (*Figure 2C*). Finally, a piece of tissue was obtained from the blue contour area and sent to the pathology department to verify whether it was prostate cancer tissue (*Figure 2D*). Meanwhile, it was verified whether the tumor contour located in the overall section was completely consistent through the standard pathological section diagnostic process.

Data and statistical analysis

In this cohort study, all statistical analyses were conducted using SPSS v. 25.0 (IBM Corp., Armonk, NY, USA) and GraphPad Prism 8.0 (GraphPad Software, Inc., La Jolla, CA, USA). The measurement data that did not conform to the normal distribution are summarized as median with upper and lower quartiles [M (Q1, Q3)]. The measurement data conforming to a normal distribution are summarized as mean and standard deviation (mean ± SD). The categorical variables are summarized as the number of cases and percentages [n (%)], and the Chi-squared test (χ^2 test) was used to compare the groups. Univariate logistic regression was used to analyze the independent influencing factors associated with positive cognitive sampling and positive 3D stereolocalization. When the negative predictive value

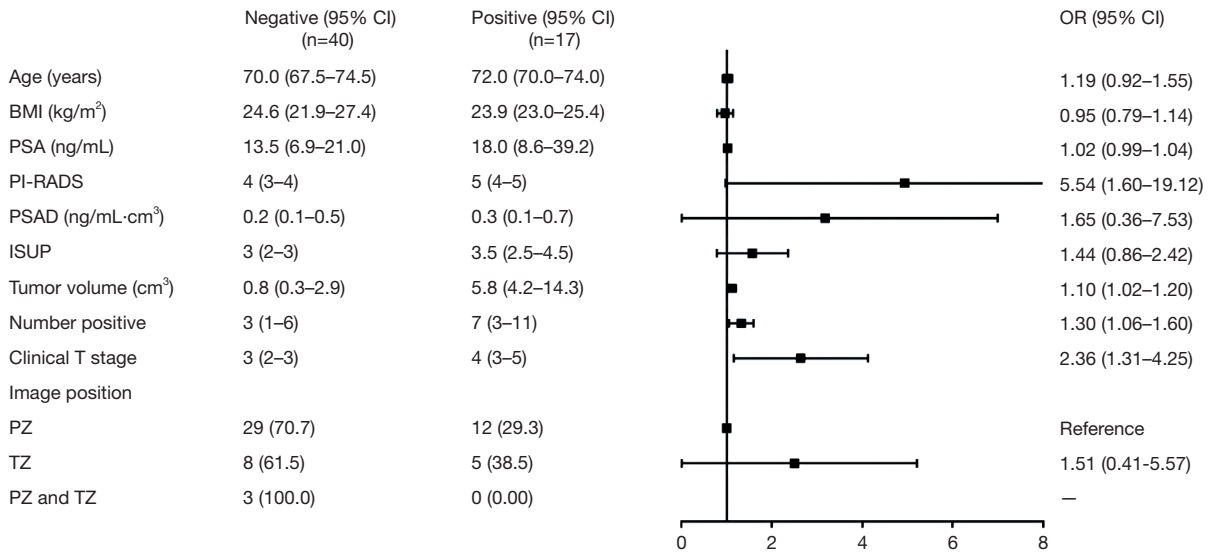

Figure 3 Logistic regression analysis was used to analyze the influencing factors of cognitive sampling in 57 cases of radical prostatectomy in The First Affiliated Hospital of Soochow University. OR, odds ratio; CI, confidence interval; BMI, body mass index; PSA, prostate-specific antigen; PI-RADS, Prostate Imaging Report and Data System; PSAD, prostate-specific antigen density; ISUP, International Society of Urological Pathology; PZ, peripheral zone; TZ, transition zone.

(NPV) of the tumor volume was 100%, the optimal cutoff was the critical value of the tumor volume at the time of negative sampling. P<0.05 denoted statistical significance.

Results

Comparison of the positive rate of cognitive sampling and 3D stereotaxic sampling

Among the 57 cases of cognitive sampling, 17 cases (29.82%) were positive, and among 54 cases of 3D stereotaxic sampling, 33 cases (61.11%) were positive. The positive rate of the 3D stereotaxic sampling was much higher than that of cognitive sampling (P=0.001).

Analysis of the influencing factors of cognitive sampling and 3D stereotaxic sampling

We analyzed the prostate-specific antigen (PSA) value, Prostate Imaging Report and Data System (PI-RADS) score, PSA density (PSAD) value, International Society of Urological Pathology (ISUP) grade, lesion image location, tumor volume, number of positive needles in preoperative diagnostic biopsy, and clinical T stage of patients, as these could affect the positive sampling rate. *Figure 3* shows that PSA, PSAD, ISUP, and lesion image location were not independent influencing factors of positive cognitive sampling. The number of positive needles, tumor volume, PI-RADS score, and clinical T stage were all independent influencing factors for cognitive sampling: more positive puncture needles was associated with greater tumor volume, higher PI-RADS score, more advanced clinical T stage, and greater likelihood of the cognitive sampling rate being positive.

Figure 4 shows that PSA, PSAD, ISUP, lesion image location, number of positive puncture needles, tumor volume, PI-RADS score, and clinical T stage were not independent influencing factors for positive sampling. Collectively, these data suggest that factors influencing cognitive sampling are eliminated in 3D stereotaxic sampling. The optimal cutoff value of tumor volume when the NPVs of both cognitive sampling and 3D stereotaxic sampling were 100% was used as the critical value of negative sampling. When the tumor volume of cognitive sampling was ≤0.41 cm^3, all samples could be considered negative; when the tumor volume of 3D stereotaxic was ≤0.26 cm^3, all samples could be considered negative. The results showed that 3D stereotaxic sampling enables the targeted extraction of significantly smaller tumors.

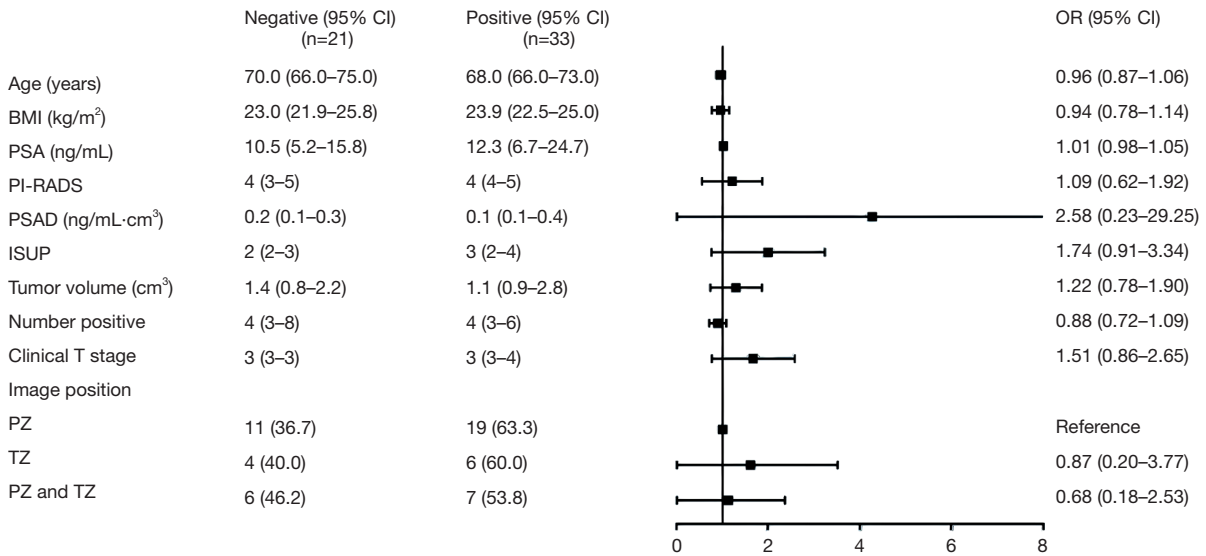

Figure 4 Logistic regression analysis was used to analyze the influencing factors of cognitive sampling in 54 cases of radical prostatectomy in The First Affiliated Hospital of Soochow University. OR, odds ratio; CI, confidence interval; BMI, body mass index; PSA, prostate-specific antigen; PI-RADS, Prostate Imaging Report and Data System; PSAD, prostate-specific antigen density; ISUP, International Society of Urological Pathology; PZ, peripheral zone; TZ, transition zone.

The learning curve for manipulating 3D stereotaxic sampling

A total of 54 cases of 3D stereotaxic sampling were assigned to the pre-, middle, and late, periods with 18 cases in each period. The positive sampling rates for the pre-, middle, and late period were 56%, 61%, and 78%, respectively. The positive rate for the sampling showed a trend of improvement and finally reached nearly 80% (*Figure 5*). The changes in the positive rates for the three periods reflected the learning curve of the sampling personnel, indicating that the 3D stereotaxic sampling method could be implemented in clinical practice through simple training. The sampling time in each period also gradually shortened. In the late period, the average sampling time was shortened to 7 minutes, which is half the duration of the pre-period (*Figure 6*).

Discussion

The boundary between prostate cancer tissue and normal prostate tissue is not clear. Additionally, prostate tumor tissue often has a multifocal scattered distribution, generally does not produce cancerous interstitial reaction, and is difficult to distinguish by the naked eye. Formaldehyde-fixed paraffin embedding (FFPE) tissue is the most commonly used method for tissue preservation (12). However, with the rapid development of second-generation sequencing (SGS) and third-generation sequencing (TGS), several studies on prostate cancer research require tumor tissue samples and have high requirements for the collection and preservation of specimens. RNA sequencing and other technologies require at least 30 minutes of acquisition and preservation; otherwise, the nucleic acid can easily degrade, leading to reduced quality and research failure. Timely cryopreservation at –80 ℃ or in liquid nitrogen can effectively prolong the duration of preservation. However, the acquisition of prostate cancer specimens has been markedly hindered in research due to the limitations of the operating room and inconvenient pathological verification, among other factors.

To facilitate the accurate and rapid acquisition of prostate cancer tissue *in vitro* and meet the high requirements of prostate cancer research for tumor tissue acquisition, our study combined the mpMRI data of patients using 3D modeling and printing technology to locate prostate cancer tumor tissue *in vitro* to more precisely sample prostate cancer. The 3D sampling device demonstrated repeatability and meets the requirements of research for the specimen acquisition methods needed for prostate cancer research and provided the rapid acquisition of prostate

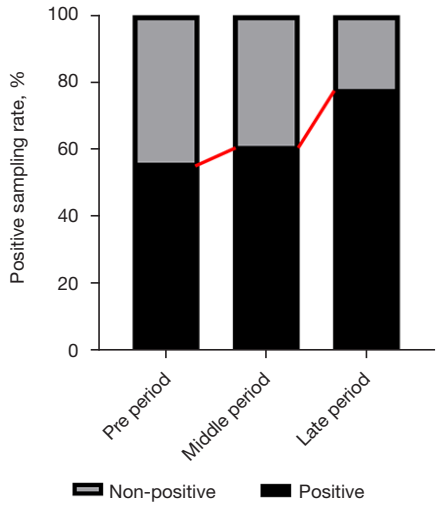

Figure 5 Positive sampling rate of three-dimensional stereotaxic localization in three different periods.

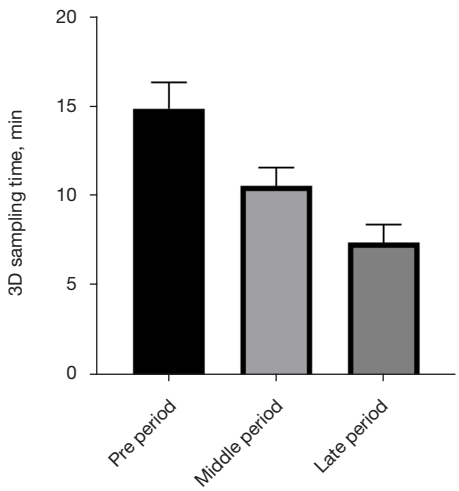

Figure 6 Comparison of sampling time of three-dimensional stereotaxic localization in three periods. The sampling time of the pre-, middle, and late period were 14.83±1.47, 10.5±1.05, and 7.33±1.03 min, respectively. Data are presented as the mean ± standard deviation.

cancer lesions. Additionally, after simple cleaning, it can be reused for the next specimen. The results of this study showed that the positive rate for the cognitive sampling method is critically low in clinical practice and affected by various factors. The number of positive needles used for preoperative prostate puncture, tumor volume, PI-RADS score, and clinical T stage were related to the positive rate

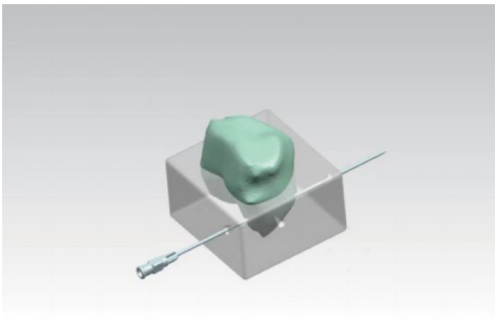

Figure 7 Individualized three-dimensional printing positioning model.

of sampling. Moreover, studies have shown that higher number of positive needles, greater tumor volume, higher PI-RADS score, and higher clinical T stage are associated with a greater likelihood of acquiring prostate cancer tissue and can lead to bias. Through the 3D stereotaxic sampling in our study, the positive rate was significantly improved, and the factors that originally had significant effects on cognitive sampling were eliminated. There were no significant differences in the number of positive needles used for preoperative prostate puncture, tumor volume, PI-RADS score, or clinical T staging between the negative and positive groups of 3D stereotaxic sampling. Moreover, the tumor volume range of 3D stereotaxic sampling was larger than that of cognitive sampling. In this study, the distance between the puncture needles was 5 mm. Therefore, a maximum cross-section diameter of the tumor of less than 5 mm led to certain systematic errors, and there were errors caused by the subtle movement of the prostate gland during puncture positioning. Therefore, we designed a personalized 3D stereotaxic device based on this study. The corresponding puncture positioning model was printed according to the 3D prostate model of each patient. The device has also been patented (*Figure 7*). There have been few specific introductions on the precise sampling methods for obtaining prostate cancer tumor tissue samples from the prostate *in vitro*. Various medical centers have different sampling methods for prostate cancer tumor tissue, but specimen sampling is unavoidable.

3D printing technology has been used to print precise the anatomical models of the human organs to be treated (13). With high specificity and sensitivity, mpMRI is currently

internationally recognized as the best imaging method for the diagnosis of prostate cancer. T2-weighted imaging combined with diffusion-weighted imaging has been shown to significantly improve the detection rate of clinically meaningful prostate cancer (Gleason score ≥6 and focal diameter >6 mm) (14). Siddiqui *et al.* combined MR with an ultrasound fusion system for targeted puncture biopsies, improving the detection rate of high-risk prostate cancers and reducing the detection of low-risk prostate cancers (15). Similarly, Rapisarda *et al.* indicated that prostate mpMRI has good accuracy in detecting prostate cancer before biopsy (16). Therefore, the combination of 3D technology and mpMRI to locate prostate tumor tissue is promising.

Moreover, artificial intelligence (AI) is a computer science field aimed at creating intelligent devices that perform tasks that currently require human intelligence. In machine learning, deep learning models enable computers to learn by example, and AI is revolutionizing healthcare. When applied to diagnostic imaging, AI has shown great accuracy in detecting prostate lesions and predicting patient survival and treatment response (17). Clinical decision support systems (CDSS) are being developed to provide improvements in decision-making. Currently, machine learning and deep learning technologies for prostate cancer diagnosis and care are based on the clinical application of CDSS with limited data. Therefore, AI and machine learning are still considered growing fields (17,18).

According to our study, the sampling positive rate of 3D stereotaxic sampling was nearly 80%, which confirms the accuracy of 3D stereotaxic sampling. The 20% missed detection rate may be accounted for by the mpMRI itself missing the prostate or the prostate cancer lesions being too small to be sampled. In addition, the size of the prostate in mpMRI might not have been consistent with that in the isolated prostate due to edema. To solve this problem, we can calculate the ratio of the lesion boundary to the whole specimen boundary in advance, and then locate the tumor boundary in the isolated prostate in equal proportion.

Conclusions

3D stereotaxic sampling of prostate cancer tissue can ensure the accuracy and convenience of sampling, reduce the errors caused by the cognitive sampling of prostate cancer lesions, and eliminate the interference of a series of influential factors such as the PSA value, lesion size, lesion image location, and clinical T staging. This method has the advantages of convenience, low cost, and high repeatability, but it also has the disadvantages of preoperative localization and complicated calculations. In the future, the combination of mpMRI and AI can be used to automate and program prostate cancer tumor tissue sampling, which is the final blueprint of sampling research, to facilitate scientific research on prostate cancer.

Acknowledgments

Funding: This work was supported by the Jiangsu Provincial Key Research and Development Program (Nos. BE2020655 and BE2020654), the General Program of Jiangsu Health Commission (No. H2019040), the Gusu Health Personnel Training Project of Suzhou City (No. GSWS2019033), the National Natural Science Foundation of China (Nos. 32200533, 82002715, 81472401, and 81772708), and the Natural Science Foundation of Jiangsu Province (No. BK20190170).

Footnote

Reporting Checklist: The authors have completed the STROBE reporting checklist. Available at https://qims.amegroups.com/article/view/10.21037/qims-23-1820/rc

Conflicts of Interest: All authors have completed the ICMJE uniform disclosure form (available at https://qims.amegroups.com/article/view/10.21037/qims-23-1820/coif). The authors have no conflicts of interest to declare.

Ethical Statement: The authors are accountable for all aspects of the work in ensuring that questions related to the accuracy or integrity of any part of the work are appropriately investigated and resolved. This study was conducted in accordance with the Declaration of Helsinki (as revised in 2013). All patients were counseled about the risks of the procedure, and they signed an informed consent form that included permission to use their clinical data for research. Ethical approval was obtained from the Institutional Review Board of The First Affiliated Hospital of Soochow University (No. [2022]469).

References

1. Carter HB, Albertsen PC, Barry MJ, Etzioni R, Freedland SJ, Greene KL, Holmberg L, Kantoff P, Konety BR, Murad MH, Penson DF, Zietman AL. Early detection of prostate cancer: AUA Guideline. J Urol 2013;190:419-26.
2. Jones JS. Saturation biopsy for detecting and characterizing prostate cancer. BJU Int 2007;99:1340-4.
3. Jones JS. Prostate Cancer: Are We Over-Diagnosing-or Under-Thinking? Eur Urol 2008;53:10-2.
4. Yang X, Monn MF, Liu L, Liu Y, Su J, Lyu T, Gong Y, Wang L, Davidson DD, Cheng L. Incidental prostate cancer in Asian men: high prevalence of incidental prostatic adenocarcinoma in Chinese patients undergoing radical cystoprostatectomy for treatment of bladder cancer and selection of candidates for prostate-sparing cystectomy. Prostate 2015;75:845-54.
5. Tóth E, Salamon F. Prostate cancer reporting: needle biopsy and radical prostatectomy specimen. Magy Onkol 2019;63:10-5.
6. Dash A, Maine IP, Varambally S, Shen R, Chinnaiyan AM, Rubin MA. Changes in differential gene expression because of warm ischemia time of radical prostatectomy specimens. Am J Pathol 2002;161:1743-8.
7. Boesen L. Multiparametric MRI in detection and staging of prostate cancer. Dan Med J 2017;64:B5327.
8. Drost FH, Osses DF, Nieboer D, Steyerberg EW, Bangma CH, Roobol MJ, Schoots IG. Prostate MRI, with or without MRI-targeted biopsy, and systematic biopsy for detecting prostate cancer. Cochrane Database Syst Rev 2019;4:CD012663.
9. Klotz L, Chin J, Black PC, Finelli A, Anidjar M, Bladou F, Mercado A, Levental M, Ghai S, Chang SD, Milot L, Patel C, Kassam Z, Moore C, Kasivisvanathan V, Loblaw A, Kebabdjian M, Earle CC, Pond GR, Haider MA. Comparison of Multiparametric Magnetic Resonance Imaging-Targeted Biopsy With Systematic Transrectal Ultrasonography Biopsy for Biopsy-Naive Men at Risk for Prostate Cancer: A Phase 3 Randomized Clinical Trial. JAMA Oncol 2021;7:534-42.
10. Tack P, Victor J, Gemmel P, Annemans L. 3D-printing techniques in a medical setting: a systematic literature review. Biomed Eng Online 2016;15:115.
11. Shin T, Ukimura O, Gill IS. Three-dimensional Printed Model of Prostate Anatomy and Targeted Biopsy-proven Index Tumor to Facilitate Nerve-sparing Prostatectomy. Eur Urol 2016;69:377-9.
12. Rivero ER, Neves AC, Silva-Valenzuela MG, Sousa SO, Nunes FD. Simple salting-out method for DNA extraction from formalin-fixed, paraffin-embedded tissues. Pathol Res Pract 2006;202:523-9.
13. Michiels C, Jambon E, Sarrazin J, Boulenger de Hauteclocque A, Ricard S, Grenier N, Faessel M, Bos F, Bernhard JC. Comprehensive review of 3D printing use in medicine: Comparison with practical applications in urology. Prog Urol 2021;31:762-71.
14. Haider MA, van der Kwast TH, Tanguay J, Evans AJ, Hashmi AT, Lockwood G, Trachtenberg J. Combined T2-weighted and diffusion-weighted MRI for localization of prostate cancer. AJR Am J Roentgenol 2007;189:323-8.
15. Siddiqui MM, Rais-Bahrami S, Turkbey B, George AK, Rothwax J, Shakir N, Okoro C, Raskolnikov D, Parnes HL, Linehan WM, Merino MJ, Simon RM, Choyke PL, Wood BJ, Pinto PA. Comparison of MR/ultrasound fusion-guided biopsy with ultrasound-guided biopsy for the diagnosis of prostate cancer. JAMA 2015;313:390-7.
16. Rapisarda S, Bada M, Crocetto F, Barone B, Arcaniolo D, Polara A, Imbimbo C, Grosso G. The role of multiparametric resonance and biopsy in prostate cancer detection: comparison with definitive histological report after laparoscopic/robotic radical prostatectomy. Abdom Radiol (NY) 2020;45:4178-84.
17. Tătaru OS, Vartolomei MD, Rassweiler JJ, Virgil O, Lucarelli G, Porpiglia F, Amparore D, Manfredi M, Carrieri G, Falagario U, Terracciano D, de Cobelli O, Busetto GM, Del Giudice F, Ferro M. Artificial Intelligence and Machine Learning in Prostate Cancer Patient Management-Current Trends and Future Perspectives. Diagnostics (Basel) 2021;11:354.
18. Klarenbeek SE, Weekenstroo HHA, Sedelaar JPM, Fütterer JJ, Prokop M, Tummers M. The Effect of Higher Level Computerized Clinical Decision Support Systems on Oncology Care: A Systematic Review. Cancers (Basel) 2020;12:1032.

Cite this article as: Li W, Ling Z, Chen X, Wang C, Guo Y, Bao J, Huang R, Wei X. A modified sampling method for the precise detection of prostate cancer tissues using a three-dimensional stereotaxic location technique. Quant Imaging Med Surg 2024;14(9):6724-6733. doi: 10.21037/qims-23-1820

